Research Article Vol. 16, No. 2 / 1 Feb 2025 / Biomedical Optics Express 426
Biomedical Optics EXPRESS

Soft elastomeric optical fibers for oxygen change measurements of blood and living tissues: a thermoplastic polyurethane assessment

MIGUEL LLERA,[1,*] EDITH LAUX,[1] FRÉDÉRIC FLAHAUT,[1] LAURE JEANDUPEUX,[1] ESTEBAN ALVAREZ SEOANE,[1] MAXIME ZERBIB,[2] JEAN-CHARLES BEUGNOT,[2] AND PHILIPPE POTTY[1]

[1]*Haute Ecole Arc Ingénierie, Haute Ecole Spécialisée de Suisse Occidentale, Rue de la Serre 7, 2610 Saint-Imier, Switzerland*
[2]*Institut FEMTO-ST, CNRS Université de Franche-Comté, ENSMM Sup Microtech, Besançon 25030, France*
[*]*Miguel.llera@he-arc.ch*

Abstract: This paper discusses the design, fabrication, and use of thermoplastic polyurethane optical fibers intended for oxygen saturation measurements. It includes an evaluation of the fiber attenuation and the creation of two probes for the measurement assessment. For comparison, a third probe is made using conventional glass optical fibers. The assessment is conducted in two stages: first, absorption measurements are performed using a mixture of methylene blue and intralipid diluted in deionized water; second, a measurement with human blood is conducted to demonstrate the effectiveness of such fibers in measuring blood oxygen saturation. Additionally, a comprehensive study of measurement stability is provided.

1. Introduction

Optical fiber spectroscopy (OFS) has garnered significant interest for decades. Studies using glass fibers [1] were published even before Kao and Hockman published their landmark work presenting a possible medium for transmitting optical frequencies [2]. OFS application in the medical field have substantial implications for in vivo evaluations. These measurements can be classified into distinct categories, including Raman spectroscopy, fluorescence spectroscopy, diffuse reflectance spectroscopy, and fiber oximetry, among others. The goal of these techniques is to improve diagnostic capabilities, monitor disease progression, and evaluate treatment efficacy, ultimately enhancing human health.

Fiber oximetry is a well-established OFS technique that involves measuring blood oxygen saturation using multiple optical fibers [3]. In tissue oximetry, two components are identified and quantified: cytochrome c oxidase and hemoglobin. Both components absorb light in specific bands within the near-infrared spectrum and exist in two forms: reduced (oxygen-depleted) and oxidized (oxygen-saturated). Each form has a different absorption spectrum. By employing two distinct wavelengths, it is possible to separately measure the relative proportions of reduced hemoglobin (HHb) and the oxidized hemoglobin (oxyhemoglobin, HbO_2), thus determining whether a tissue is hypoxic or not.

Tissue oxygen saturation measurement has shown potential detecting cancers, including ovarian cancer [4]. Different types of ovarian cancer can be classified based on the tissue involved. Malignant ovarian tumors are mainly of epithelial origin, developing in the outer layer of the ovary. Stromal tumors arise from the ovary's supporting tissue and have a low malignant potential. Germ cell tumors originate from the ovary's germ cells and constitute approximately 5% of ovarian cancers [5,6]. Cancer cells can multiply, invade and damage nearby tissues [7]. They

#549790 https://doi.org/10.1364/BOE.549790
Journal © 2025 Received 22 Nov 2024; revised 27 Dec 2024; accepted 27 Dec 2024; published 6 Jan 2025

Biomedical Optics EXPRESS

can invade blood and lymphatic vessels stimulating new blood vessels formation to supply the nutrients needed for growth and survival. As malignant cells proliferate, the tissue structure changes. Ovarian cancer tissue has been shown to have increased vascularization compared to healthy tissue but reduced oxygen saturation. This tumor hypoxia alters the tissue's optical characteristics, detectable by oximetry. The tumor hypoxia results in alterations in the optical characteristics of the tissue, which can be detected by oximetry.

To improve the effectiveness of surgical debulking for malignant tissue and potentially avoid the complete ovary removal, a rapid, in vivo and reliable analysis method is required. Consequently, research into optical spectroscopy methods has intensified in recent years. Various solutions have been explored, including those allowing analysis without tissue sampling. The objective of these methodologies is to obtain real-time information. Among the evaluated spectroscopic methods are approaches based on vibrational spectroscopy such as FT-IR (Fourier Transform Infrared Spectroscopy) and Raman spectroscopy [8], NIR (near infrared) spectroscopy [9,10], and MIR (mid infrared) spectroscopy [11]. However, these methods are typically conducted ex vivo and require sophisticated instrumentation.

To avoid tissue sampling, using of optical fibers to measure localized oximetry is not new. For example, optical fibers with small prisms were used to measure oxygen levels on an esophageal wall [12]. Another example is the evaluation of oximetry measurements on intestinal walls for chronic mesenteric ischemia [13], where T-Stat 303 probes from Spectros were employed. Most fiber optic oximeters use a bundle of glass optical fibers to collect enough light from the remote tissue location [14]. These bundles have limitations for certain applications because direct contact between the fibers and tissue can cause injuries due to the stiffness of the glass. Also, the large diameters used prevent the bundle from being placed in small areas, such as for ovarian cancer detection, or in tubular structures such as blood vessels. This has led to the emergence of alternative oximetry methods. Optoelectronic catheters encapsulated in soft biocompatible materials have been proposed to avoid using stiff glass optical fibers [15]. However, the absence of an optical fiber necessitates placing the light-emitting diodes and photodiodes directly at the probe's tip, resulting in a final diameter of 1.5 mm which limits its use in small locations. Polymer optical fibers, proposed in [16–18], offer reduced stiffness compared to glass fibers but still have high stiffness and large diameters. One approach to using more flexible materials is to develop wearable fiber-based oximeters for real-time healthcare monitoring. In [19] a flexible and transparent polyethylene terephthalate (PET) substrate and Poly(3,4-ethylenedioxythiophene)-poly(styrenesulfonate) (PEDOT:PSS), a transparent conducting material, were used to create a wearable clothing-type pulse oximeter. However, this solution is not designed for internal use where miniaturization is essential to intimate optical interactions with biological tissues or blood. For this purpose, new studies are exploring the use of bioresorbable materials, which offer promising solutions in terms of biocompatibility and flexibility. In [20], waveguides with cores made of monocrystalline silicon encapsulated with poly(lactide-co-glycolide) (PLGA) to act as the cladding were produced. Although these waveguides can be used for oximetric measurements, their size and fabrication complexity limit their ease of use. A recent study proposed a new bioresorbable optical fiber made of calcium phosphate glass (CFG) [21] which can be as small as to a few hundred micrometers. While miniaturization is achievable, the stiffness of the CFG can be problematic when intimate contact with human tissues is required.

To address miniaturization and softness issues, a new type of optical fiber has emerged in recent years: elastomeric optical fibers. These materials have a Young's modulus that is much closer to that observed in natural tissues [22] allowing them to contact human tissues without causing damage. Thermoset polymers, as silicone, are interesting but the produced fibers with such elastomers can only be realized by molding, limiting the final dimensions to a certain range. To easily produce large quantities of fibers in various dimensions and structures, thermoplastic elastomers must be used. Thermoplastics offer the possibility to fabricate preforms with complex

Biomedical Optics EXPRESS

designs that can be thermally drawn to smaller dimensions. Several studies were realized using such materials [23–27], but most focus on the development of the fibers themselves or for basic measurements, leveraging their high deformability. In this manuscript, we propose using thermoplastic polyurethane (TPU) optical fibers to produce oximetric sensors for oxygen saturation measurement. We first evaluate their effectiveness through spectroscopic absorption measurements using methylene blue as the absorption medium. Three fiber probes are fabricated and compared: two glass optical fibers, two TPU fibers, and a new 3-core TPU fiber. The 3-core TPU fiber aims to offer further miniaturization compared to the two TPU fibers. A final measurement of hemoglobin oxygenation changes in human blood demonstrates the utility of TPU fibers to perform oximetric measurements. To the best of our knowledge, this is the first time that elastomeric optical fibers are used for such measurements. The manuscript is organized as follows: We first describe the fabrication of the fibers and probes and their basic characterization. The experimental setup for spectroscopic absorption measurement and the corresponding signal processing are then explained before presenting the transmittance results for the three probes. Subsequently, we present the results of blood absorption, followed by a discussion highlighting the potential and limitations of these fibers for oximetric applications. The manuscript ends with a conclusion.

2. Optical fibers and probes fabrication

Three distinct fiber optic probes were produced. One probe was constructed using fused silica fibers, a second using two TPU optical fibers, and a third using a 3-core TPU optical fiber. This section outlines the fabrication procedures for the fibers and probes and provides optical characterization data specific to the TPU fibers. Except for the 3-core fiber, the design of the probes comprises one optical fiber for transporting light from the source to the measurement area (illumination fiber) and a second fiber for conveying the reflected light from the measurement area to the detection unit (detection fiber). In the case of the 3-core fiber probe, the design incorporates a single 3-core TPU fiber, with the individual cores connected to discrete fused silica fibers via a homemade fan-in/fan-out (FIFO) device. Subsequently, the separated fibers can be connected to the pertinent optical source or detection unit.

2.1. Fused silica optical fibers

Figure 1(a) and 1(b) show the fused silica probe schematically and visually. The illumination fiber employs a 1-meter-long step-index optical fiber (Thorlabs FG050LGA) with dimensions of 50/125/250 µm (core diameter/cladding diameter/coating diameter). The detection fiber employs a 1-meter-long step-index optical fiber (Thorlabs FG105LCA) with dimensions of 105/125/250 µm. Both fibers are uncoated over a 4-cm length and then precisely cleaved using an LDC-400 cleaver (Vytran). The fibers are simultaneously inserted into a glass capillary with dimensions of 300/794 µm (internal/external diameter) to ensure close proximity and parallel alignment. The two fiber endfaces are aligned at approximately 1-2 mm from the capillary output. Finally, adhesive is applied at both capillary ends to prevent any liquid penetration and any fiber movement. On the opposite side of the fibers, FC-APC connectors are mounted (Thorlabs 30126A9) to enable optical connection with other components.

2.2. TPU single core optical fibers

2.2.1. Optical fibers fabrication and characterization

The TPU optical fiber fabrication process follows the same procedure as previously described in our work [23]. We have slightly improved our drawing tower by adding a glass crucible inside the original graphite crucible. This change allows a better diameter matching between the preform and the heating crucible allowing a smoother fiber diameter stability during the

Biomedical Optics EXPRESS

Fig. 1. Schematic view of the fused silica probe (a) and visual view of the fused silica probe tip (b).

drawing process. The initial preform is produced through injection molding and then thermally drawn to create thin optical fibers. In our case, the illumination and detection fibers are produced using the same preform, which has a 10 mm core diameter as illustrated in Fig. 2. The core is nearly invisible within the preform due to a lensing effect that brings its diameter to a level close to the external preform diameter when viewed transversally. The TPU preform materials are Ellastollan 1185A10 for the core and Ellastollan 1185A for the cladding, both provided by BASF. The external diameter of the preform is 15 mm, with a useful length of 8-9 cm. The refractive indexes for the BASF materials 1185A10 and 1185A are 1.537 and 1.505, respectively. In Fig. 3, we can see the endfaces of two optical fibers that were produced by thermally drawing this preform. The left part shows the fiber illuminated with an external light source, whilst the right part illustrates the fiber guiding white light. The final fiber diameters are approximately between 111/168 µm (core/cladding) and 118/176 µm. These fibers were used to fabricate the single-core TPU optical fiber probe.

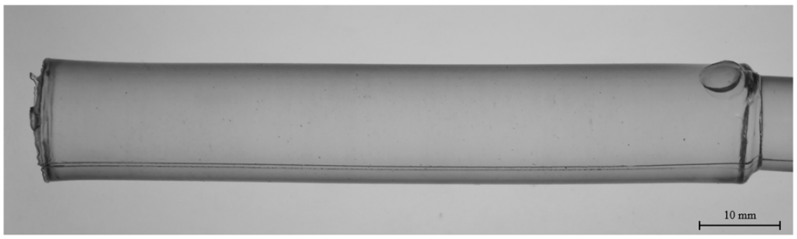

Fig. 2. TPU preform of 10 mm core diameter and 15 mm cladding diameter.

Attenuation of the fibers was measured on two separate fibers having similar diameters as those used for the probe using the cut-back technique from 40 cm down to 20 cm with a sampling length of 2 cm. The diameter of the samples exhibited maximum fluctuations of approximately 20 µm, or 10% of the fiber diameter. Due to these diameter fluctuations and the softness of the materials, we have limited the measurements to two as we can only measure a loss tendency. In [23] we discussed this issue, noting that any loss measurement will always be very unstable due to any fiber movement or enface quality change. Therefore, repeating more measurements is unnecessary. The optical source was a SuperK COMPACT fiber laser (NKT Photonics), with a spectrum ranging from 450 nm to 2400 nm. The detection was realized using an optical spectrum analyzer (OSA) SR-6N1000-100 (Ocean Optics), which has a spectrum bandwidth ranging from 600 nm to 1250 nm. Following each cut, the OSA was used to measure the transmitted light

Biomedical Optics EXPRESS

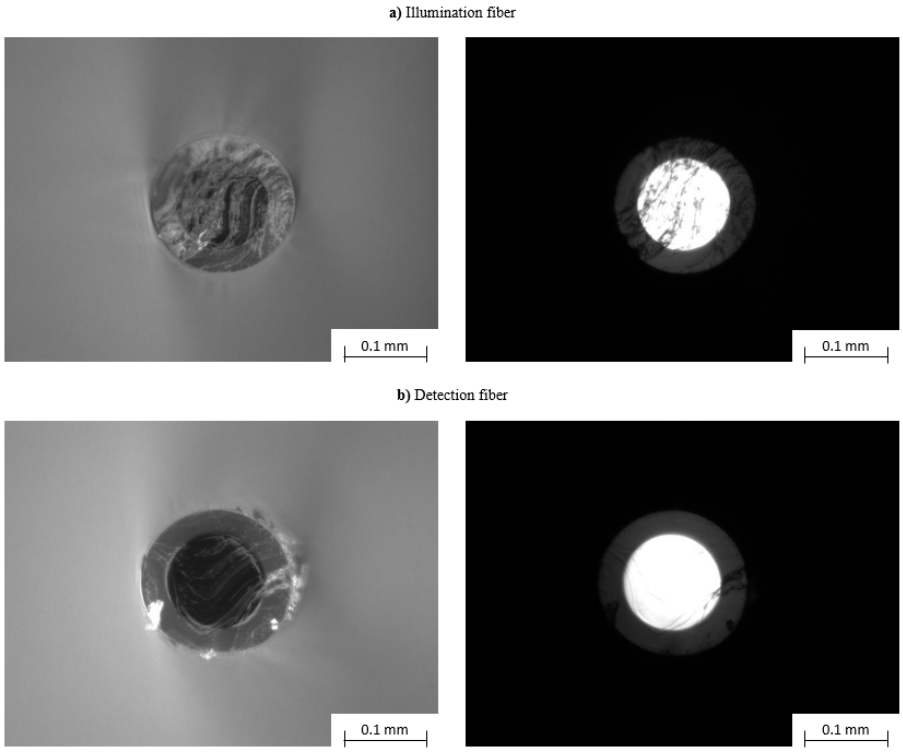

Fig. 3. Single core TPU fibers endfaces: a) Illumination fiber, b) detection fiber.

power for the full spectrum. The attenuation losses at each wavelength were determined by linear regression of the transmitted power variation during each cut-back step. The results are presented in Fig. 4, which also includes a third curve representing the average of the two measurements. We decided to limit the upper wavelength to 1100 nm because the results above this wavelength do not show enough power to be reliable. As shown, there are two low attenuation windows: 600–900 nm and 970–1000 nm. The optical loss of these low-attenuation windows is approximately 0.2 dB/cm and 0.25 dB/cm, respectively. The absorption band we can observe between 900–970 nm can potentially originate from water absorption [28]. In [29], we have already observed an attenuation increase starting around 900 nm for another TPU: Elastollan 1160D (BASF). This supports the assumption that this loss may relate to a common material absorption within TPUs and not to a waveguide effect. Rayleigh scattering can also be observed in the spectrum from 800 nm down to 600 nm. Here also, we can see that the measured losses between the two measurements differ by roughly 0.05 dB/cm. The discrepancy can be attributed to two main factors: the inherent uncertainty of the measurement process itself and the inherent differences in the fibers themselves, such as variations in fiber diameter or the presence of wrinkles on the core/cladding interface.

2.2.2. Probe fabrication

Figure 5(a) and 5(b) show the single core TPU optical fiber probe schematically and visually. Given the higher optical attenuation of TPU optical fibers compared to fused silica optical fibers, it is necessary to keep them short, typically in the range of a few tens of cm. This means that the TPU fiber needs to be connected to a fused silica optical fiber that connects either to the optical source or to the detection system. In our case, we have decided to keep the TPU fiber length

Biomedical Optics EXPRESS

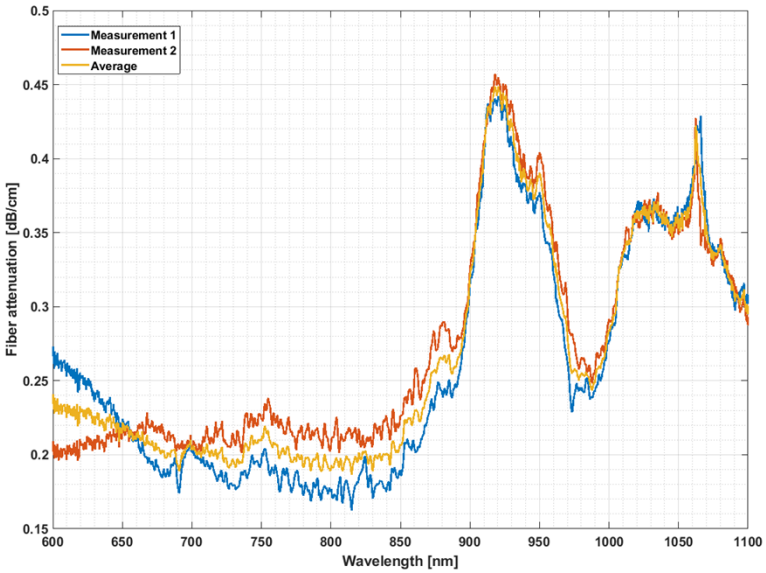

Fig. 4. Single core TPU fiber attenuation measurement vs wavelength.

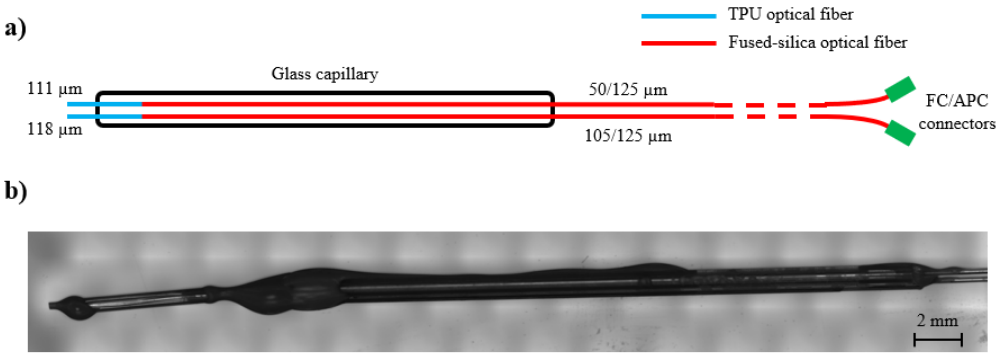

Fig. 5. Schematic view of the single core TPU probe (a) and visual view of the single core probe tip (b).

down to 2 cm. The procedure for mounting the probe is illustrated in Fig. 6. The initial step (a) is to align a TPU optical fiber with its corresponding fused silica fiber using an LFS-4000 splicer (Vytran): 50/125 µm (Thorlabs FG050LGA) for the illumination fiber and 105/125 µm (Thorlabs FG105LVA) for the detection fiber. Once the alignment is complete, the fibers are joined together using a UV adhesive. The alignment is then protected inside a fused silica capillary (b) with dimensions 300/794 µm (internal and external diameter – Molex part number: 1068150069). The second TPU optical fiber and its corresponding fused silica fiber are prepared in the same manner (c). The alignment is secured and safeguarded within a fused silica capillary. As for the silica probe, to ensure a proper light recollecting into the detection fiber, the two TPU fibers need to be close in contact to each other. For that, two approaches can be used: thermally welding the two fibers together as a ribbon or using another capillary to align the two fibers inside. To simplify our process, we have decided to use the capillary method. In this instance, we have used a short portion (~1 cm) of fused silica capillary with dimensions 536/660 µm (internal and external diameter – Molex part number: 1068150476) (d). By allowing the TPU optical

Biomedical Optics EXPRESS

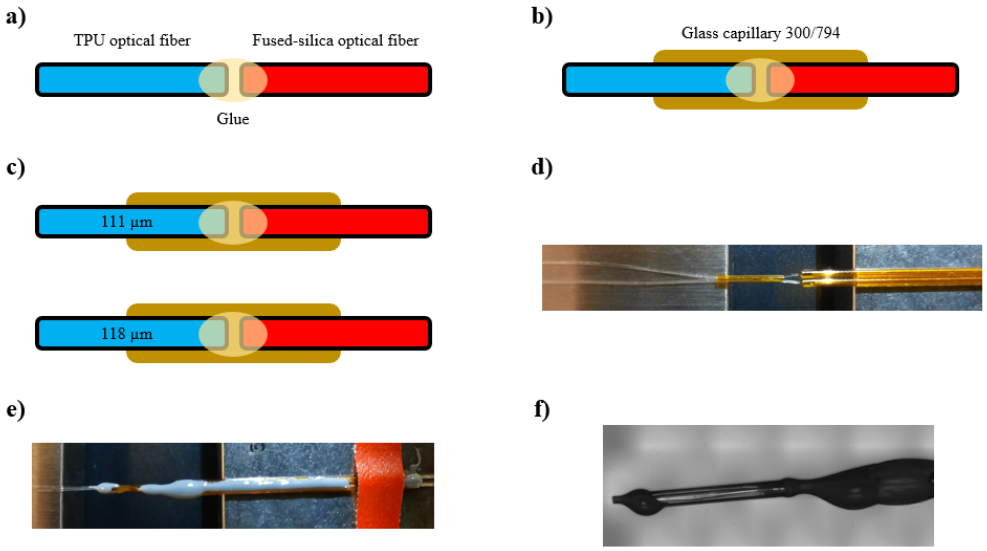

Fig. 6. Single core TPU probe mounting process. a) TPU to fused silica fiber alignment and gluing b) TPU to fused silica fiber alignment protection with a fused silica capillary c) second fiber preparation d) alignment of the two TPU fibers into a glass capillary e) probe gluing f) TPU optical fibers cut at ∼1 mm out of the glass capillary.

fibers to extend just 1 mm beyond the capillary end, we can maintain a parallel alignment and ensure proximity, facilitated by the capillary's internal diameter. Some applications may require a longer length than 1 mm, given the need for TPU softness. However, the aforementioned welding technique or the use of a TPU capillary, instead of fused silica, can effectively address this issue, enabling the fabrication of significantly longer TPU probes. To prevent any movement of the fibers, we have glued them at the capillary ends (e). The fabrication of the probe is completed with the cutting process of the TPU fibers at 1 mm length (f). On the opposite side of the fibers, FC-APC connectors (Thorlabs 30126A9) are mounted to facilitate an optical connection with other components.

2.3. TPU 3-core fiber

2.3.1. Optical fibers fabrication and characterization

The fabrication of TPU 3-core optical fibers follows the same procedure as for single-core fibers, except that the preform must have three cores instead of one. For a single core preform, the core is produced by a 2 steps injection process: 1) A cylindrical metallic insert is positioned along the mold axis to create a hollow preform after injection. 2) A second TPU is then injected into the preform, with a refractive index higher than that of the hollow preform. For the 3-core fibers, three spatially separated cores are required within the same preform. The process is carried out in accordance with the established procedure for a traditional single core preform, except that distinct metallic inserts are positioned separately within the mold during the first injection. Subsequently, for the cores injection, a second TPU is injected simultaneously into each hollow preform hole, after removing the corresponding insert. This ensures an optimal polymer penetration. As the 3-core fiber is intended for oximetric use, only two cores are required: a detection core and an illumination core. The second illumination core in our fiber could be useful for reference purposes in different applications, and it also helps to equilibrate the pressures inside the preform during the injection process. The core sizes are 3 mm for the illumination cores and 7 mm for the detection core, with a preform diameter of 15 mm. Figure 7 illustrates a

Biomedical Optics EXPRESS

cross-sectional view of a preform (a) and a front view (b). As for the single core fibers, the TPU preform materials are Ellastollan 1185A10 for the core and Ellastollan 1185A for the cladding with the same refractive indexes. In Fig. 8, we can see the endfaces of a 3-core fiber that was produced by thermally drawing this preform. The left part shows the fiber illuminated with an external light source, whilst the right part shows the fiber when guiding white light. The final fiber diameters are approximately 35-40 µm for the illumination cores (n° 1-2), 80-90 µm for the detection core (n° 3), and 190-210 µm for the external diameter.

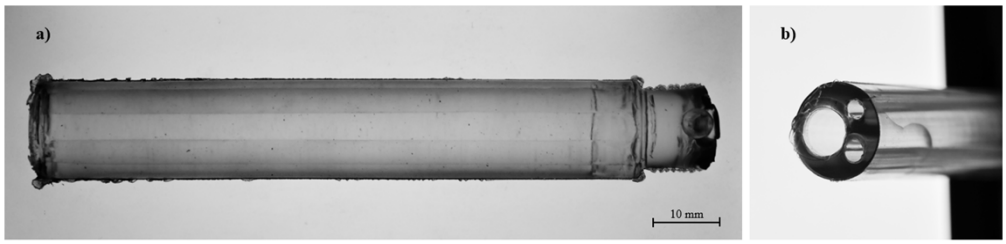

Fig. 7. 3-core fiber preform: (a) lateral view (b) front view.

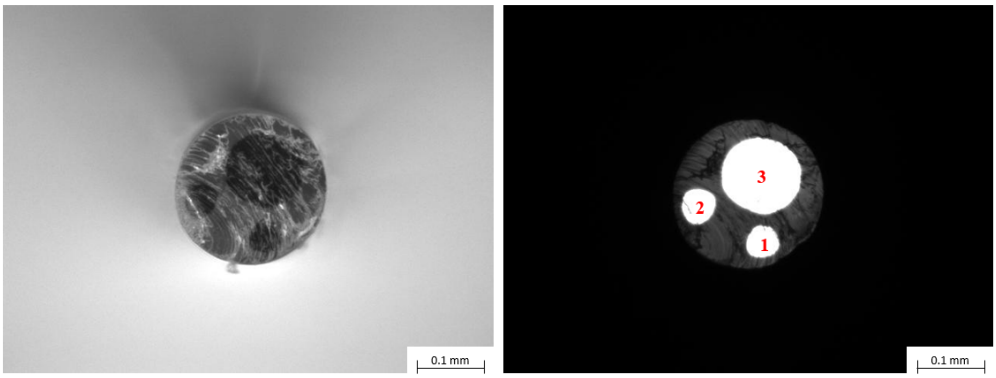

Fig. 8. 3-core fiber endface: left, external lightning; right, light guiding with cores numbering.

The fiber attenuation was measured using the same procedure as for the single core fibers. We measured only the cores n°1 and n°3, and only once. The attenuation curves can be seen in Fig. 9. Since the TPU materials are identical to those used for the TPU single core fibers, we also observe similarities in the attenuation spectrum pattern, particularly in the absorption band between 900 and 970 nm. Nevertheless, a significant difference is seen in the main attenuation, which is higher than for the single core fiber. Additionally, core n°3 exhibits a higher level of attenuation compared to core n°1. The higher attenuation observed in core n°3 can likely be attributed to the presence of more lossy higher modes propagating in a larger core diameter compared to the n°1 [30]. The discrepancy observed between the core n°1 and the single core fiber, whose core diameter is larger, suggests that the 3-core fiber may experience additional attenuation due to its waveguide structure. The presence of three cores in the preform may generate additional stresses during fabrication and thermal drawing, resulting in a rougher core/cladding interface and a deviation from a pure circular core. This can be observed by zooming in on the endfaces of the 3-core fiber and the single-core fiber, as illustrated in Fig. 10.

Biomedical Optics EXPRESS

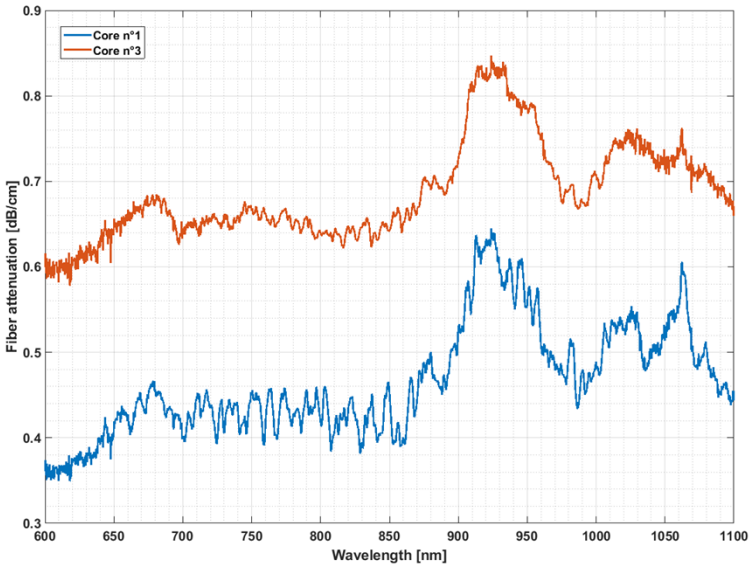

Fig. 9. Attenuation curve for a 3-core fiber for the cores n°1 and n°3.

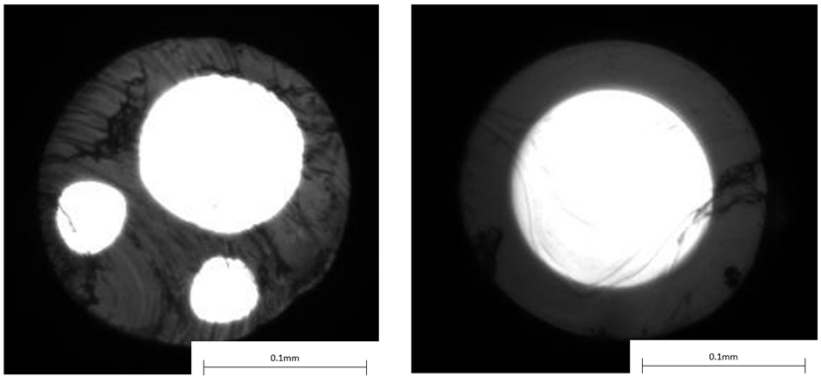

Fig. 10. 3-core fiber (left) and single core fiber (right) endfaces comparison.

2.3.2. Probe fabrication

Figure 11 shows the 3-core TPU optical fiber probe schematically and visually. Like the single core TPU probe, the 3-core fiber needs to be kept short due to its higher attenuation compared to single core fibers. After careful consideration, we decided to maintain a length of 5 cm for the 3-core TPU optical fiber probe, as this length provided sufficient signal strength. The 3-core TPU probe's primary requirement is the use of a FIFO component, which facilitates the interconnection of single fused silica fibers to the various cores of the 3-core TPU fiber. The design of the 3-core TPU fiber allows for a simple solution. If the 3-core TPU fiber is kept close to an external diameter of 200 µm, the three cores are aligned in a triangular pattern, similar to aligning three 80 µm external diameter fused silica fibers in a triangular pattern. Figure 12 provides a schematic representation of this concept, illustrating the superposition of a 3-core fiber endface on three fused silica fibers with 80 µm external diameters.

The FIFO production requires 80 µm fibers, but most commercial fused silica optical fibers with such diameters have core diameters not exceeding 10 µm. This is insufficient for our probe,

Biomedical Optics EXPRESS

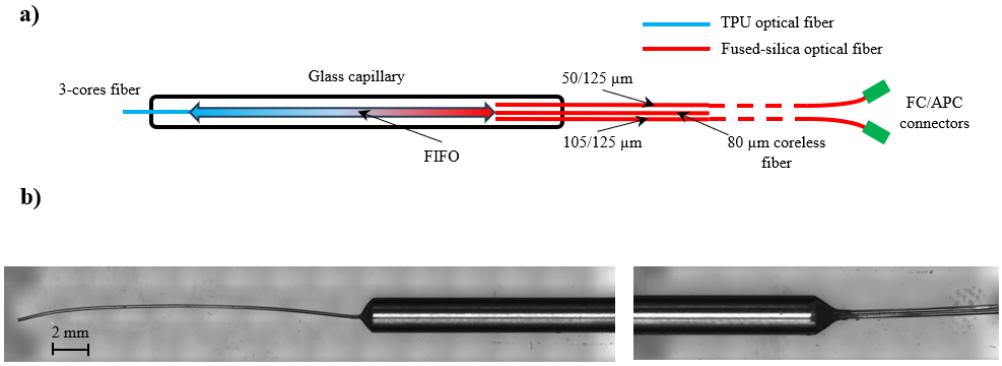

Fig. 11. Schematic view of the 3-core TPU probe (a) and visual view of the 3-core TPU probe (b).

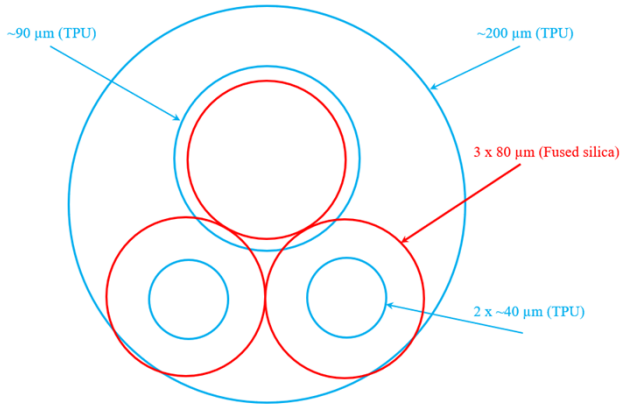

Fig. 12. Schematic view of the superposition of 80 µm fused silica fibers on a 3-core TPU fiber.

as we require larger diameters to maximize light delivery to the sensing area and to optimize the detection of light at the probe's tip. To address this, we tapered fibers with dimensions 100/140 µm (Nexans Switzerland – 1990) down to ~57/80 µm using a heat-brush technique. Specifically, the method of manufacturing fiber tips is adapted from a conventional optical fiber tapering process for the fabrication of high transmission nanofibers [31,32]. The heat-brush technique consists of holding the 100/140 µm fiber on two plates and lighting a flame underneath to raise the temperature of the silica to its softening point. The controlled movement of the translation plates is then engaged to reduce the diameter of the fiber as it lengthens. This technique makes it possible to design tapers with predefined shapes and lengths. For the fiber tips tapering, the target diameter was 80 µm for the cladding, corresponding to a core of approximately 57 µm. The final step involves manually cleaving the taper and validating its transverse dimensions using an optical microscope. This process enabled us to produce two tapered fibers with dimensions exceeding 2 cm in length. The two fibers served as the basis for the development of the FIFO and probe. The fabrication process for the probe is illustrated in Fig. 13. It begins by splicing the tapered fibers (on the untapered side) to their corresponding fused silica fibers: 50/125 µm (Thorlabs FG050LGA) for the illumination fiber and 105/125 µm (Thorlabs FG105LVA) for the detection fiber (a). FC-APC connectors are mounted (Thorlabs 30126A9) on the other side of these fibers to allow an optical connection with other components (b). The FIFO part is

Biomedical Optics EXPRESS

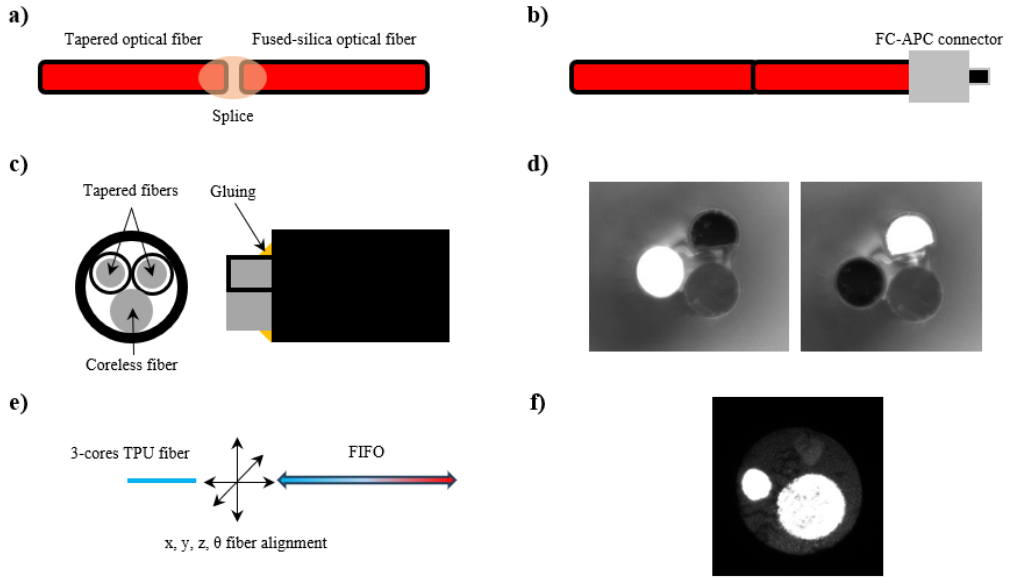

Fig. 13. 3-core TPU fiber probe mounting process. a) Splicing of tapered fibers with standard fibers (b) Mounting of FC-APC connector at the standard fiber end (c) Mounting the tapered fibers end + one 80 µm coreless fiber into a fused silica capillary of dimensions 180/350 µm + gluing (d) visual check of the light continuity (e) Alignment of the FIFO end to the 3-core fiber entrance (f) Visual check that cores n°1 and n°3 are correctly aligned

completed by inserting both tapered fibers (on their taper side) into a fused silica capillary with dimensions 180/350 µm (Molex part number: 1068150025) and by adding a third fiber to create the final triangular alignment: a 5 cm length 80 µm coreless fiber (Exail IXF-CORELESS-80) (c). It is essential to ensure that the three fibers extend 1-2 mm beyond the capillary and are securely glued in place to maintain optimal alignment. An optical test is conducted to ensure that the FIFO is functioning correctly for both tapered fibers (d). The most critical step is to properly align the FIFO with the 3-core TPU fiber. This process is completed using an LFS-4000 splicer (Vytran), which allows four-axis alignment on each fiber holder. Optimal alignment is achieved when the two cores (1 and 3) can be illuminated separately with maximum intensity (f). The final step is to safeguard the FIFO and its alignment with the 3-core fiber. This is done by first affixing the FIFO connection to the 3-core fiber and then encapsulating the FIFO and its connection with a metallic capillary with dimensions 0.63/2 mm (Interalloy L-HL 0002905), as illustrated in Fig. 11(b).

3. Absorbance measurements

To evaluate the suitability of our TPU fibers for oximetric measurements and potentially other spectroscopic applications, we first conducted absorbance measurements on methylene blue with intralipid. Next, we performed measurements using outdated samples of packed red blood cells provided by local blood donation centers. For both absorbance media, the measurement setup was the same except the liquid container (methylene blue or blood). Signal processing differs for the methylene blue compared to the blood.

Biomedical Optics EXPRESS

3.1. Methylene blue

3.1.1. Measurement setup

Methylene blue is a salt used as a dye or as a medication. Intralipid is an emulsion of water and fat that is commonly used in tissue phantoms to produce a light scattering environment [33]. Methylene blue absorbs light in the visible spectrum, with an absorbance peak centered near 670 nm. This peak corresponds to the deoxyhemoglobin (HHb) absorbance increase observed below the isosbestic point HHb makes with the oxyhemoglobin (HbO_2) absorbance at ~805 nm. The measurement setup is illustrated in Fig. 14. A broadband source (SuperK COMPACT – NKT Photonics) launches a supercontinuum white light (450–2400 nm) through the various probes described in chapter 2. The probe output is inserted into a spectroscopic cuvette (Semadeni 8857) filled with a mix of methylene blue (> 82%, Sigma-Aldrich M9140) and intralipid (20% emulsion, Sigma-Aldrich I141) diluted in deionized water (standard purity). The diffused and reflected light is then collected by the probe and sent back to the OSA (SR-6N1000-100 – Ocean Optics). After measuring the spectra, a signal processing procedure is applied to determine the absorbance of methylene blue at different concentrations.

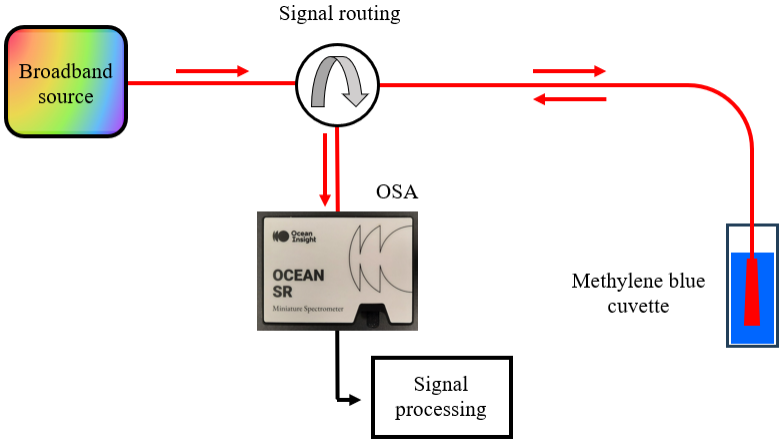

Fig. 14. Measurement setup for methylene blue absorbance.

The methylene blue and intralipid concentrations were prepared as follows. To determine the absorptive properties of methylene blue at defined concentrations, we used series of dilutions of intralipid in deionised water, with a concentration of 10%. The methylene blue concentrations were 3.1 µmol/l, 6.1 µmol/l, 12 µmol/l, 23.2 µmol/l, and 35.2 µmol/l. The mixtures were pipetted into transparent macro-UV-vis spectroscopy cuvettes. Additionally, a separate mixture without methylene blue was prepared as a reference point for zero absorption. To eliminate any external light interference, the cuvette was placed in a black housing during the measurement process. The optical probes were immersed in the solution, with the tip positioned approximately midway through the solution.

3.1.2. Signal processing

The signal processing used to quantify the methylene blue absorbance is described hereafter. Each measurement uses a different integration time for which the OSA produces a specific background spectrum. Therefore, for every measurement, this background spectrum was removed to the measured spectrum before proceeding the signal processing. It should be noted that the different spectra measured at varying methylene blue concentrations may also exhibit varying levels of intensity. These intensity variations are dependent on the occurrence of varying losses

Biomedical Optics EXPRESS

along the different fibers and components or the reflection of some light inside the cuvette. To ensure consistency, it is essential to normalize each measured spectrum, $I_i(\lambda)$, and the reference spectrum, $IR(\lambda)$, at a wavelength λ outside the methylene blue absorption band. The index i corresponds to the various concentrations of methylene blue. We selected a wavelength of 800 nm for normalization, which is well outside the absorption red tail, ending around 750 nm. Thus, the normalized spectra $NI_i(\lambda)$ used to perform the absorbance calculus, and the normalized reference spectrum $IRN(\lambda)$ are given by

$$NI_i(\lambda) = I_i(\lambda)/I_i(800) \tag{1}$$

$$IRN(\lambda) = IR(\lambda)/IR(800) \tag{2}$$

We can now calculate easily the absorbance as

$$A_i(\lambda) = \log 10\left(\frac{IRN(\lambda)}{NI_i(\lambda)}\right) \tag{3}$$

To represent values in a linear way, we decided to express the transmittance, in percentage, which can be calculated by using the absorbance $A_i(\lambda)$ as

$$T_i(\lambda) = 10^{-A_i(\lambda)} \cdot 100\% \tag{4}$$

3.1.3. Experimental results

The transmittance measurements using our three probes are shown in Fig. 15. We can observe that all three probes were able to measure a transmittance but there is a slight magnitude increase when using the TPU's probes. The 3-core TPU probe demonstrates the most significant increase in measured transmittance and the noisier measurement. It is not possible to attribute these differences directly to the higher attenuation observed for the TPU fibers, since each probe measures a reference spectrum that already incorporates the losses induced by the probe itself. However, an explanation relates the higher attenuation of the TPU fibers with this result: if the light intensity outgoing from the probe is reduced, the depth of the optical path that the light interacts with to generate sufficient reflected or scattered light to be coupled back to the OSA is also reduced. Therefore, it can be concluded that the differing transmittances observed between the probes are solely attributable to a change in light intensity interacting with the intralipid and methylene blue mixture. The additional losses that the TPU probes are facing are as follows: attenuation of TPU fibers, coupling losses between TPU fibers and fused silica fibers, and for the 3-core TPU optical fiber, the FIFO.

To evaluate the uncertainty of the measurements realized with the methylene blue, we conducted three different analyses. First, we evaluated the OSA stability. We measured the background noise given by the OSA $BN_j\ (\lambda)$ every minute for 1 hour and with a 0.6s integration time that corresponds to the longest integration time used during the experiments. Index j relates to the measurement number. We then took measurement $BN_1\ (\lambda)$ as the reference and subsequently divided each measurement by $BN_1\ (\lambda)$. If there is no spectral change or any drift, we would get a perfect horizontal line centered in the ordinate at 1. We then subtracted 1 to the results and multiply by 100% to get the variation of the background signal over 1 hour for all wavelength steps. To determine the overall standard deviation, we discarded $BN_1\ (\lambda)$ that has a standard deviation of 0% for any wavelength step. Results are shown in Fig. 16 where we can see all the intensity variations over the period in % (a) and the resulting standard deviation at 1σ (b). The uncertainty remains slightly above ±1%.

As a second analysis we evaluated the optical source stability. Here, the output of our broadband source was directly connected to the OSA but with reduced power to avoid the OSA saturation. Then, we measured the spectrum every minute for 1 hour and with a 0.6s integration time. The

Biomedical Optics EXPRESS

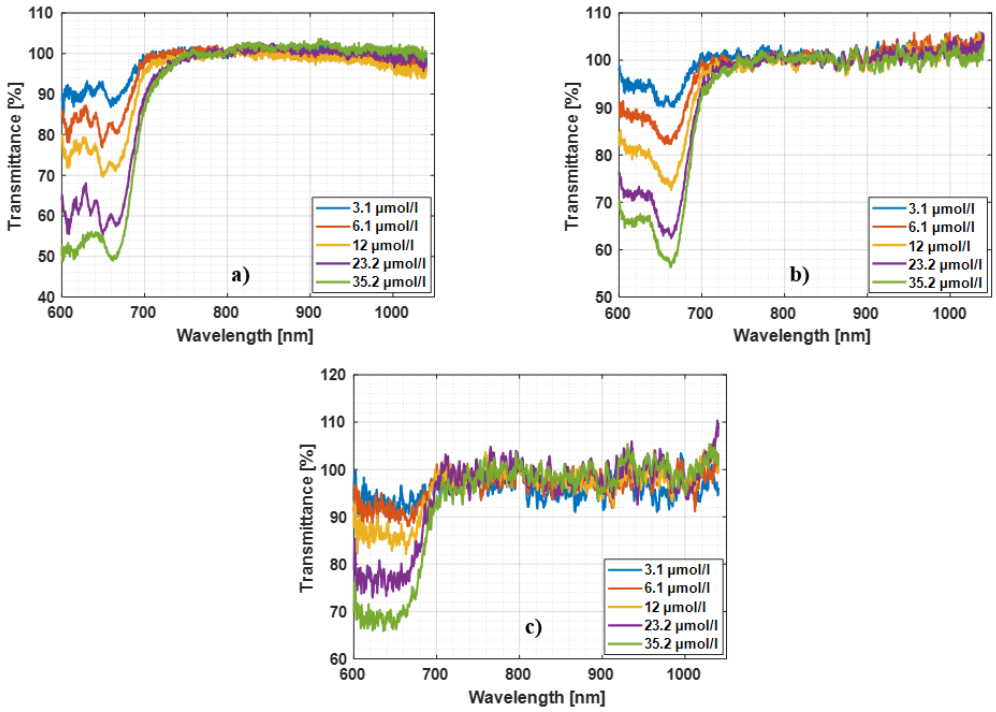

Fig. 15. Transmittance spectra for three probes. a) fused silica b) two single core TPU c) 3-core TPU.

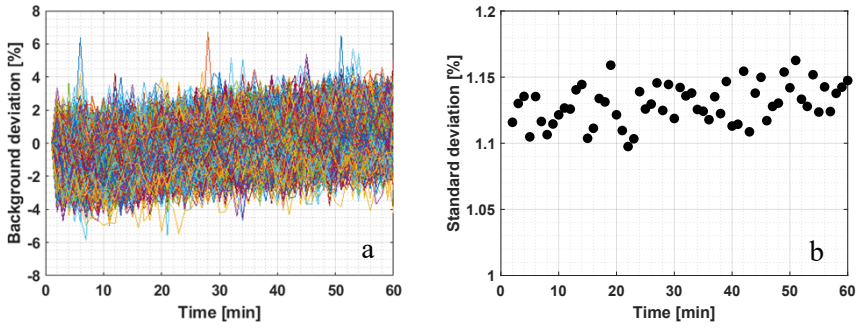

Fig. 16. Stability measurement for the OSA. (a) background spectrum intensity deviation [%] and (b) the standard deviation [%].

Biomedical Optics EXPRESS

subsequent steps to determine the uncertainty are the same as for the OSA and we take the first measured spectrum as reference. Results are shown in Fig. 17 where we can see all the intensity variations over the period in % (a) and the resulting standard deviation at 1σ (b). The uncertainty is slightly increasing with time but remains around ±1% over the measurement period.

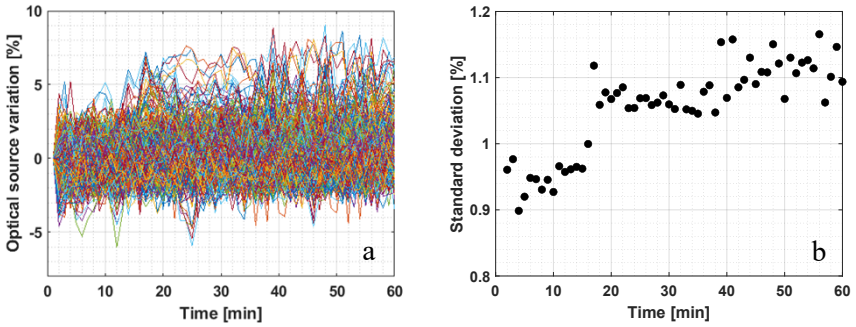

Fig. 17. Stability measurement for the optical source. (a) background deviation [%] and (b) the standard deviation [%].

The third and last analysis can directly be performed using the measurements shown in Fig. 15. We may assume that there is a negligible absorbance occurring in the spectral window 800–1000 nm, giving a transmittance stable at 100%. However, even if the measurements remain around 100% of transmittance, they exhibit noisy behavior. We have decided to use this part of the signal to measure the uncertainty on the measured transmittance. For each methylene blue concentration, we determined the standard deviation along the spectral range considered. Figure 18 shows the standard deviation for the three probes versus the methylene blue concentration. The uncertainty for the silica probe remains around ±1%, indicating it is mainly driven by the OSA and optical source uncertainties. For the TPU probes, as could be expected, the uncertainty increases to ±1.5% when using the TPU single core probe and increases to ±2.5% for the 3-core TPU probe.

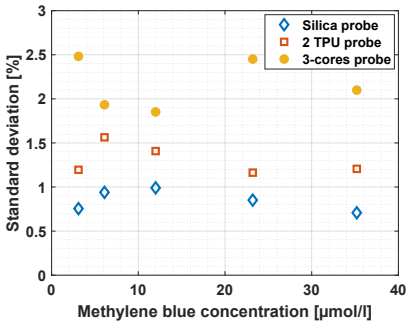

Fig. 18. Uncertainty measurement for the three probes versus methylene blue concentration.

3.2. Red blood cells

In human bodies the transport of oxygen in the blood is realized by the red blood cells, or erythrocytes, whose cytoplasm is primarily composed of hemoglobin molecules. Hemoglobin is an iron-containing biomolecule that can bind oxygen with a capacity of 1.34 mL of O_2 per gram. Most of the oxygen required by the body is transported by hemoglobins that exist in both the T-state (low level of affinity to oxygen) and the R-state (high level of affinity to oxygen). Each erythrocyte state exhibits a distinct spectral absorbance. This difference forms the basis of the

Biomedical Optics EXPRESS

oximetry principle, whereby the presence of deoxyhemoglobin (HHb) below the isosbestic point of ~805 nm dominates the absorbance, whereas oxyhemoglobin (HbO_2) dominates above this point.

3.2.1. Setup preparation

The packed erythrocytes were prepared as follows. An outdated blood bag, previously separated from blood-plasma and stabilised with an additive CPD solution (citrate phosphate dextrose) as part of the blood donation process, was used. The volume of the bag was approximately 300 ml at a hematocrit level of 60-70%. For our experiments, approximately 45 ml of erythrocytes (AB+) were removed from the bag and placed in a 250 ml round-bottom flask. Figure 19 illustrates the flask and its surrounding environment. The flask was tempered at 36.8 °C and N_2 was bubbled in the erythrocytes through one of the flask necks via a syringe with a flow rate of 110 ml/min for 15 minutes. To avoid damaging the cells, only gas stream and its bubbles were used to mix the blood. During the N_2 bubbling, the main entrance of the flask was closed with an output gas tubing. For the absorbance measurement, a rubber stopper with two drilled holes was used. The two drilled holes served two distinct purposes. The first hole was used to secure the fiber probe, whilst the second hole facilitated airflow between the flask and the surrounding environment. After 15-minute N_2 application, the output gas tubing was removed, and the rubber stopper was immediately placed. The fiber probe used in this experiment was the two single core TPU. Once the probe was introduced at a depth of ~ 1 cm in the oxygen-depleted erythrocytes, the optical spectra were recorded every minute for 3 hours using the setup described in Fig. 14 with the round-bottom flask instead of the cuvette. Over the course of three hours, the erythrocytes gradually regained their normal oxygenation level as they interacted with the air inside the round-bottom flask.

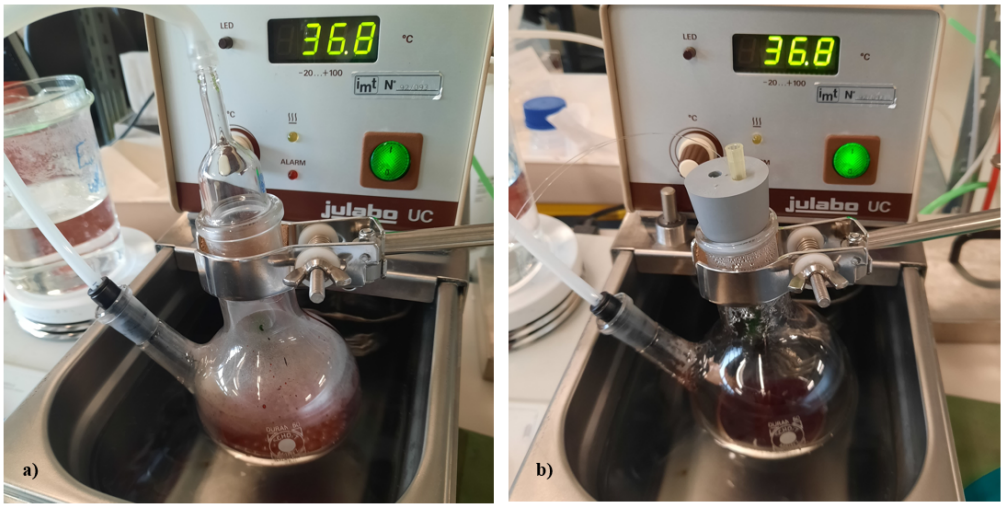

Fig. 19. Blood deoxygenation setup. a) deoxygenation with output gas tubing. b) Output gas tubing is removed and replaced with the rubber stopper. The single core TPU probe fits through it.

3.2.2. Signal processing and experimental results

The signal processing used to quantify the erythrocytes absorbance is described as follows. A spectrum is recorded every minute for 3 hours. As for the methylene blue measurement, the different spectra measured may exhibit varying intensity levels. Therefore, it is essential to

Biomedical Optics EXPRESS

normalize each spectrum at a specific wavelength. As blood is known to have an isosbestic point at ~805 nm, we first perform the normalization at this wavelength. To identify any possible wavelengths at which the absorbance remains constant, we have taken three measurements close to the beginning (time = 0 h) and three others close to the end (time = 3 h) and plotted them. Figure 20 illustrates these 6 normalized spectra measured at time = 0 h and 3 h, which clearly demonstrate the presence of wavelengths for which no absorbance change occurred, indicated by the red circles. We can identify two spectral windows that can be used to realize an oximetric measurement easily: "B" between the red circles n°1 and n°2, and "E" after the red circle n°4. Following this initial observation, we have decided to change the normalization wavelength to the wavelength of red circle n°2 as it offers a less noisy spectrum than 805 nm. Once the spectra are normalized, we can trace the intensity variation at two specific wavelengths located in the spectral windows "B" and "E". The spectra shown in Fig. 20 highlight, the usefulness of a broadband optical source instead of using the traditional wavelengths for oximetry, i.e. 660 nm and 940 nm. This is crucial because, with these new elastomeric optical fibers, we must find the right wavelengths for oximetric measurements. TPU fibers have a different attenuation spectrum compared to the standard glass optical fibers, which may render traditional wavelengths ineffective. For this measurement, we did not subtract the background spectrum, as was done for the methylene blue experiment. The reason is that we kept the OSA running and used the same integration time, resulting in a constant background spectrum with an uncertainty of ±1%. As we will see in the Fig. 21, this is a well below intensity variation compared to the intensity shift induced by the erythrocytes state changes.

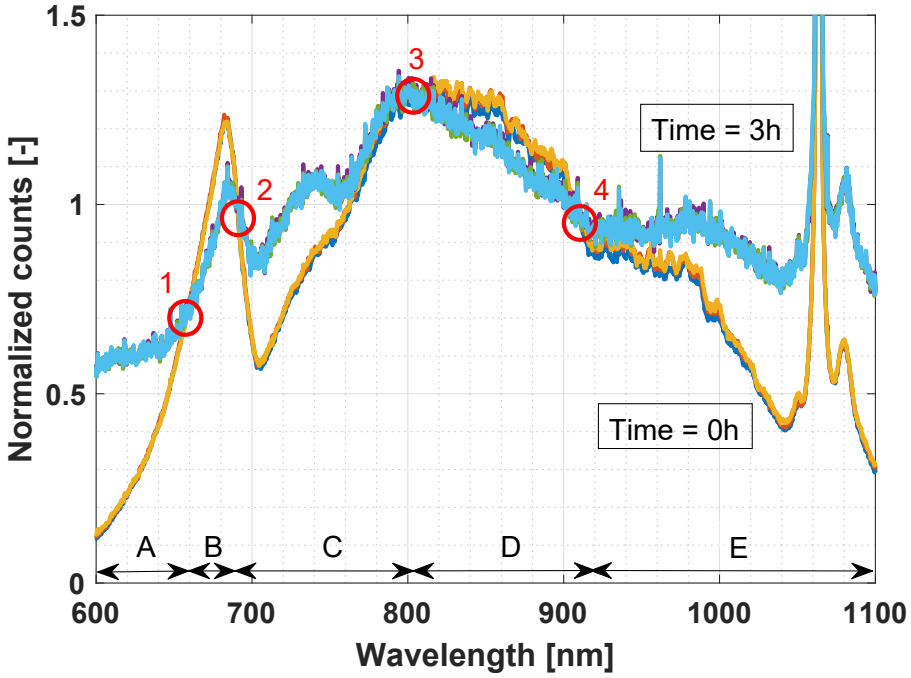

Fig. 20. Spectra recorded at 0 and 3 hours for a slow oxygenation of deoxygenated erythrocytes.

The measured spectra are dependent on both the absorbance and scattering of the erythrocyte medium, and both evolve during the measurement due to changes in hemoglobin properties. Packed erythrocytes see their HbO_2 proportion fall with time mainly due to limited gas exchange with the environment. In our case, the erythrocytes used were predominantly of the HHb state

Biomedical Optics EXPRESS

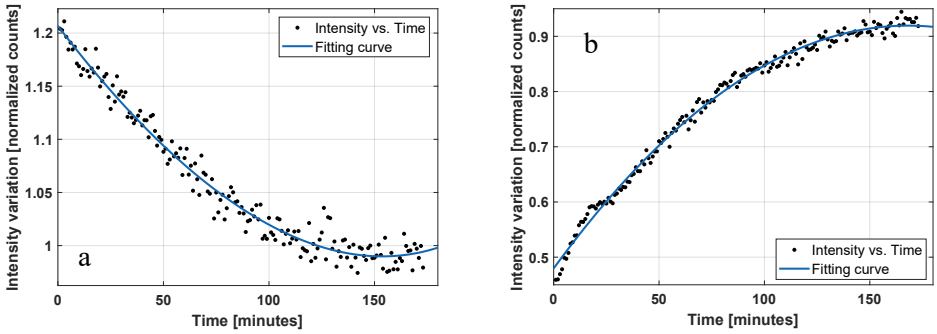

Fig. 21. Intensity variation at wavelengths 680 nm (a) and 1085 nm (b) during a 3 h oxygenation.

because they were taken out from an outdated bag. Nevertheless, a certain proportion of HbO_2 should remain and N_2 bubbling should change this state to another proportion. Analysing the spectral changes observed in Fig. 20 after N_2 bubbling, we can explain some of these differences. Spectral window "A" is most likely dominated by the presence of methemoglobin (MetHb) which is known to be produced by the reaction of hemoglobin with nitrogen compounds [34]. MetHb is the oxidized deoxy form of hemoglobin to which oxygen cannot bind. MetHb is then formed at the expense of HbO_2. However, MetHb formation at the expense of HHb is possible because HHb is more prone to oxidation under certain conditions that an outdated preservation may have increased. MetHb has a stronger absorption than HbO_2, explaining the loss of light intensity in this spectral window and confirming the presence of HbO_2 in our bag before the bubbling. The red circle n°1 wavelength corresponds to the MetHb isosbestic point with the HHb located around 660 nm [35]. Since both hemoglobin states, MetHb and HHb, dominate after bubbling and since we expect a very slow recovery of a certain HbO_2 proportion, this steady absorbance state dominates along the process even after the MetHb reduction where the MetHb half-life is of 55 minutes [36]. Spectral window "B" and red circle n°2 are a bit more challenging to understand but may be related again to the presence of MetHb. After red circle n°1, absorption of MetHb is less than that of HHb. Therefore, if some HHb is converted to MetHb, the absorption is lower than before bubbling. Red circle n°2 roughly coincides with the minimum absorption of MetHb and should correspond to the wavelength at which the effect observed in window "B" is no longer possible and light attenuation starts again to dominate after the N_2 bubbling. Therefore, spectral window "C" corresponds to the spectral range where the MetHb absorbance should dominate. Red circle n°3 corresponds to the 805 nm isosbestic point. Spectral window "D" corresponds to the spectral part where the absorbance of HHb, HbO_2 and MetHb follow a similar trend and ends at red circle n°4 where HHb absorbance begins to decrease compared to MetHb and HbO_2 [35]. We observe an increase in intensity in spectral window "E" from red circle n°4, which corroborates the fact that MetHb vanishes with time. Additionally, we know that light scattering is increasing above 805 nm and with an increase in hemoglobin oxygenation [37]. This can add intensity in the tendency we observe in spectral window "E".

Intensity variations measured in spectral windows "B" and "E" are shown in Fig. 21. For the spectral window "B", the chosen wavelength was 680 nm (a) and for the window "E", we used 1085 nm (b). To facilitate the appreciation of the variation tendency, both graphs have been fitted with a two-term exponential function. It is evident that the two measurements exhibit an inverse but analogous trend. For the 680 nm wavelength measurement, the wavelength shift is about -20% whereas it is of about +40% for the 1085 nm wavelength. Considering the previously measured overall uncertainty of the probe of ±1.5%, we can conclude that the measured intensity

Biomedical Optics EXPRESS

shifts are much greater, demonstrating that an oximetric measurement is fully realizable with the TPU fibers.

4. Discussion

The objective of this study was to demonstrate the viability of performing absorption measurements using elastomeric optical fibers that offer extreme softness compared to standard glass optical fibers or traditional polymer optical fibers made of PMMA. Furthermore, our research has demonstrated that more sophisticated TPU fibers, such as the 3-core fiber, can also be used for such measurements. For medical applications, this represents a significant advance in the ability to make measurements in highly sensitive areas or organs, where the use of glass optical fibers would be inadvisable. The significantly higher attenuation observed in TPU optical fibers compared to fused silica restricts their applications to specific distances. Nevertheless, for numerous applications, distances of just a few to tens of centimeters would suffice, or even shorter distances if only the fiber tip is required, as may be the case for ovarian cancer detection. Furthermore, the proposed fibers and their fabrication are still in the early stages of development, with the potential for additional improvements that could help to reduce the overall attenuation observed. It is also important to note that only one fiber, or core, has been used to collect light back to the OSA. The use of fiber bundles would allow for the collection of more light in the case of single-core fibers. In this regard, single-core fibers may already be a viable option, given the comparable results achieved in comparison to fused silica fibers for the methylene blue experiments. 3-core fibers may seem unsuitable for use in a fiber bundle. However, they have the potential to be valuable in extremely small areas, such as veins or capillaries, where the size of a fiber bundle would present significant challenges. We believe that the solutions proposed have the potential to be applied in several interesting and highly useful ways. The 3-core fiber has the potential to enable absorption measurements with a significantly reduced probe volume compared to current industry standards. Our final experiment with the N_2 bubbling of erythrocytes has proved that TPU fibers can be used for blood oxygen saturation measurements as the fibers respond perfectly in the full spectrum of interest. We must notice that our experiments didn't show specific performance in measuring the oxygen saturation that can be compared to commercial oximeters or previous fiber-based oximeters. We focused our study in proving that TPU optical fibers can be serious candidates for producing safer oximeters that would be used in very sensitive areas or can simply be a solution for a low-cost single use oximeter. Further studies would be needed to assess the performance of our probes in terms of oxygen saturation measurement accuracy, but the observed uncertainty of ±1.5% for the single core TPU probe may already provide a preliminary assessment.

In addition to its use in the presented applications, another usefulness of the 3-core TPU optical fiber can be found by leveraging the high softness of a multicore optical fiber. It is well known that multicore fibers face a crosstalk issue due to the closeness of their cores. In our particular case, the softness of TPU offers the potential for developing sensing applications that use the crosstalk property of the fiber. Essentially, any contact with the fiber can alter the crosstalk characteristics, potentially enabling the detection of multiple parameters. We have not yet had the opportunity to study these topics in relation to the measurements presented in this study, as they fall outside the scope of our current project and would require a different assessment.

5. Conclusion

In summary, we have designed and fabricated different TPU optical fibers with the aim of using them for absorption measurements, including single-core and 3-core TPU fibers. We measured their attenuation and found that the single-core fiber had a propagation loss of approximately 0.2 dB/cm, whilst the 3-core fiber had a loss ranging from 0.4 to 0.6 dB/cm. This increased attenuation in the 3-core fiber is likely due to a decline in the quality of the core/cladding interface

Biomedical Optics EXPRESS

compared to the single core fiber. This discrepancy may be caused by the injection of three separate cores during the preform fabrication process, which could introduce additional tensions and affect the smoothness of the thermal drawing.

We conducted absorption measurements using mixtures of methylene blue with intralipid and have assessed the ability to measure hemoglobin oxygenation changes in human erythrocytes. For this purpose, we designed optical probes made from three different fibers: fused silica, single-core TPU, and 3-core TPU. All probes performed well during the methylene blue measurements, although TPU showed lower measured absorbances. This lower absorbance is due to a reduced light intensity interacting with the methylene blue mixture, which decreases the total absorbance. The reduced light intensity in our mixture was attributed to additional losses associated with the TPU probes, including higher fiber attenuation, coupling loss between fused silica fibers and TPU fibers, and the use of a FIFO system to couple fused silica fibers to the 3-core fiber.

The overall uncertainty of our three probes was estimated to be ±1% for the silica probe, ± 1.5% for the single core TPU probe and ±2.5% for the 3-core TPU probe. The erythrocytes measurements demonstrated that TPU fibers are fully capable of being used in blood oxygen saturation measurements. The different absorbance effects observed during the measurement have tentatively been explained by the generation of MetHb and scattering effects occurring in the erythrocytes, rather than being a result of the fibers themselves. A final discussion was conducted, and the main results were reviewed.

Funding. Haute Ecole Spécialisée de Suisse Occidentale (115037/IA-RECHERCHE21-22, 128573/RI-PSTRAT23-06).

Acknowledgment. The authors acknowledge the support received from the Haute Ecole Spécialisée de Suisse Occidentale.

Disclosures. The authors declare no conflicts of interest.

Data availability. Data underlying the results presented in this paper are not publicly available at this time but may be obtained from the authors upon reasonable request.

References

1. M. L. Polanyi and R. M. Hehir, "In vivo oximeter with fast dynamic response," Rev. Sci. Instrum. **33**(10), 1050–1054 (1962).
2. K. C. Kao and G. Hockham, "Dielectric-fibre surface waveguides for optical frequencies," Proc. Inst. Electr. Eng. **113**(7), 1151–1158 (1966).
3. M. L. J. Landsman, N. Knop, G. Kwant, *et al.*, "A fiberoptic reflection oximeter," Pfluegers Arch. **373**(3), 273–282 (1978).
4. S. Nandy, A. Mostafa, I. S. Hagemann, *et al.*, "Evaluation of ovarian cancer: initial application of coregistered photoacoustic tomography and US," Radiology **289**(3), 740–747 (2018).
5. G. Mangili, C. Sigismondi, A. Gadducci, *et al.*, "Outcome and risk factors for recurrence in malignant ovarian germ cell tumors: a MITO-9 retrospective study," Int. J. Gynecol. Cancer **21**(8), 1414–1421 (2011).
6. D. Pectasides, E. Pectasides, and D. Kassanos, "Germ cell tumors of the ovary," Cancer Treat. Rev. **34**(5), 427–441 (2008).
7. G. Efthymiou, A. Saint, M. Ruff, *et al.*, "Shaping up the tumor microenvironment with cellular fibronectin," Front. Oncol. **10**, 641 (2020).
8. C. M. Krishna, G. D. Sockalingum, R. A. Bhat, *et al.*, "FTIR and Raman microspectroscopy of normal, benign, and malignant formalin-fixed ovarian tissues," Anal. Bioanal. Chem. **387**(5), 1649–1656 (2007).
9. V. R. Kondepati, H. M. Heise, and J. G. Backhaus, "Recent applications of near-infrared spectroscopy in cancer diagnosis and therapy," Anal. Bioanal. Chem. **390**(1), 125–139 (2008).
10. L. Kamemoto, A. K. Misra, S. K. Sharma, *et al.*, "Near-Infrared Micro-Raman Spectroscopy for in Vitro Detection of Cervical Cancer," Appl. Spectrosc. **64**(3), 255–261 (2010).
11. A. A. Bunaciu, V. D. Hoang, and H. Y. Aboul-Enein, "Applications of FT-IR spectrophotometry in cancer diagnostics," Crit. Rev. Anal. Chem. **45**(2), 156–165 (2015).
12. J. H. Phillips, R. P. Langford, S. H. Chang, *et al.*, "Evaluation of a fiberoptic esophageal pulse oximeter," *Annual International Conference of the IEEE Engineering in Medicine and Biology Society*, Minneapolis, MN, USA, 1509–1512 (2009).
13. S. Friedland, D. Benaron, S. Coogan, *et al.*, "Diagnosis of chronic mesenteric ischemia by visible light spectroscopy during endoscopy," Gastrointest. Endosc. **65**(2), 294–300 (2007).

Biomedical Optics EXPRESS

14. L. Hernández-Quintanar, D. A. Fabila-Bustos, M. Hernández-Chávez, *et al.*, "Fiber-optic pulseoximeter for local oxygen saturation determination using a Monte Carlo multi-layer model for calibration," Computer Methods and Programs in Biomedicine **187**, 105237 (2020).
15. W. Lu, W. Bal, H. Zhang, *et al.*, "Wireless, implantable catheter-type oximeter designed for cardiac oxygen saturation," Sci. Adv. **7**(7), eabe0579 (2021).
16. M. L. J. Landsman, N. Knop, G. A. Mook, *et al.*, "A fiberoptic reflection densitometer with cardiac output calculator," Pfluegers Arch. **379**(1), 59–69 (1979).
17. C. Liu, R. Correia, H. K. Ballaji, *et al.*, "Optical fibre-based pulse oximetry sensor with contact force detection," Sensors **18**(11), 3632 (2018).
18. M. Krehel, M. Wolf, L. F. Boesel, *et al.*, "Development of a luminous textile for reflective pulse oximetry measurements," Biomed. Opt. Express **5**(8), 2537–2547 (2014).
19. H. S. Lee, B. Noh, S. U. Kong, *et al.*, "Fiber-based quantum-dot pulse oximetry for wearable health monitoring with high wavelength selectivity and photoplethysmogram sensitivity," npj Flexible Electron. **7**(1), 15 (2023).
20. W. Bai, H. Yang, Y. Ma, *et al.*, "Flexible transient optical waveguides and surface-wave biosensors constructed from monocrystalline silicon," Adv. Mater. **30**(32), 1801584 (2018).
21. J. T. Pandayil, N. G. Boetti, D. Janner, *et al.*, "Proof of concept validation of bioresorbable optical fibers for diffuse correlation spectroscopy," Biomed. Opt. Express **15**(11), 6384–6398 (2024).
22. R. Akhtar, M. J. Sherratt, J. K. Cruickshank, *et al.*, "Characterizing the elastic properties of tissues," Mater. Today **14**(3), 96–105 (2011).
23. M. Llera, F. Flahaut, S. Bergerat, *et al.*, "Few-mode elastomeric optical fibers," Opt. Mater. Express **11**(7), 2288–2299 (2021).
24. X. Liu, S. Rao, W. Chen, *et al.*, "Fatigue-resistant hydrogel optical fibers enable peripheral nerve optogenetics during locomotion," Nat. Methods **20**(11), 1802–1809 (2023).
25. J. Gan, A. Yang, Q. Guo, *et al.*, "Flexible optical fiber sensing: materials, methodologies, and applications," Adv. Devices Instrum. **5**, 0046 (2024).
26. A. Stefani, I. D. Rukhlenko, A. F. J. Runge, *et al.*, "Wearable conformal fiber sensor for high fidelity physiological measurements," IEEE J. Sel. Top. Quantum Electron. **30**(6), 1–9 (2024).
27. K. Sharma, E. Morlec, S. Valet, *et al.*, "Polydimethylsiloxane based soft polymer optical fibers: From the processing-property relationship to pressure sensing applications," Mater. Des. **232**, 112115 (2023).
28. S. H. Chung, A. E. Cerussi, S. I. Merritt, *et al.*, "Non-invasive tissue temperature measurements based on quantitative diffuse optical spectroscopy (DOS) of water," Phys. Med. Biol. **55**(13), 3753–3765 (2010).
29. D. G. Maldonado-Hurtado, M. Llera, F. Flahaut, *et al.*, "Weight measurement and vibration detection sensor based on a thermoplastic polyurethane optical fiber," J. Lightwave Technol. **42**(5), 1740–1747 (2024).
30. R. Olshansky and D. A. Nolan, "Mode-dependent attenuation of optical fibers: excess loss," Appl. Opt. **15**(4), 1045–1047 (1976).
31. M. Zerbib, M. Romanet, T. Sylvestre, *et al.*, "Spin-orbit interaction in nanofiber-based Brillouin scattering," Opt. Express **31**(14), 22284–22295 (2023).
32. T. A. Birks and Y. W. Li, "The shape of fiber tapers," J. Lightwave Technol. **10**(4), 432–438 (1992).
33. P. D. Ninni, F. Martelli, and G. Zaccanti, "Intralipid: towards a diffusive reference standard for optical tissue phantoms," Phys. Med. Biol. **56**(2), N21–N28 (2011).
34. C. Toothill, "The chemistry of the in vivo reaction between haemoglobin and various oxides of nitrogen," Br. J. Anaesth. **39**(5), 405–412 (1967).
35. W. Zijlstra, A. Buursma, and W. Meeuwsen-van der Roest, "Absorption spectra of human fetal and adult oxyhemoglobin, de-oxyhemoglobin, carboxyhemoglobin, and methemoglobin," Clin. Chem. **37**(9), 1633–1638 (1991).
36. M. Olsen and G. Mc Evoy, "Methemoglobinemia induced by topical anesthetics," Am. J. Hosp. Pharm. **38**, 89–93 (1981).
37. J. M. Steinke and A. P. Shepherd, "Role of light scattering in whole blood oximetry," IEEE Trans. Biomed. Eng. **BME-33**(3), 294–301 (1986).